



**Histone H3.3 regulates mitotic progression in mouse embryonic fibroblasts**

Journal:	<i>Biochemistry and Cell Biology</i>
Manuscript ID	bcb-2016-0190.R1
Manuscript Type:	Article
Date Submitted by the Author:	21-Nov-2016
Complete List of Authors:	Ors, Aysegul; Universite Grenoble Alpes, Institute for Advanced Biosciences Papin, Christophe; Institut de Genetique et de Biologie Moleculaire et Cellulaire Favier, Bertrand ; Universite Grenoble Alpes, Institute for Advanced Biosciences Roulland, Yohan; Universite Grenoble Alpes, Institute for Advanced Biosciences Dalkara, Defne; Universite Grenoble Alpes, Institute for Advanced Biosciences Ozturk, Mehmet; Dokuz Eylul Universitesi, Izmir Biomedicine and Genome Center Hamiche, ALi; Institut de Genetique et de Biologie Moleculaire et Cellulaire Dimitrov, Stefan; Universite Grenoble Alpes, Institute for Advanced Biosciences Padmanabhan, Kiran; Institut de Genomique Fonctionnelle de Lyon, ;
Keyword:	histone variant h3.3, mitosis, Transcriptomics

SCHOLARONE™  
Manuscripts

## Histone H3.3 regulates mitotic progression in mouse embryonic fibroblasts

Aysegul Ors<sup>1,2\*</sup>, Christophe Papin<sup>3\*</sup>, Bertrand Favier<sup>4</sup>, Yohan Roulland<sup>1</sup>, Defne Dalkara<sup>1</sup>, Mehmet Ozturk<sup>5</sup>, Ali Hamiche<sup>3#</sup>, Stefan Dimitrov<sup>1#</sup> and Kiran Padmanabhan<sup>6#</sup>.

<sup>1</sup> Université Grenoble Alpes, Institute for Advanced Biosciences, INSERM U1209/ CNRS 5309, 38700 La Tronche, France

<sup>2</sup> Department of Molecular Biology and Genetics, Faculty of Science, Bilkent University, 06800 Ankara, Turkey

<sup>3</sup> Université de Strasbourg, Institut de Génétique et Biologie Moléculaire et Cellulaire (IGBMC), CNRS, INSERM, Equipe labélisée Ligue contre le Cancer, 1 rue Laurent Fries, B.P. 10142, 67404 Illkirch Cedex, France.

<sup>4</sup> Université de Grenoble Alpes, Team GREPI, Etablissement Français du Sang, EA 7408, BP35, 38701 La Tronche, France.

<sup>5</sup> Izmir Biomedicine and Genome Center, Faculty of Medicine, Dokuz Eylül University, Izmir, Turkey.

<sup>6</sup> Institut Génomique Fonctionnelle de Lyon (IGFL), Ecole Normale Supérieure de Lyon, UMR 5242, 46 Allée d'Italie, 69364 Lyon Cedex 07, France.

\*, equal contribution

#, corresponding authors: kiran.padmanabhan@ens-lyon.fr, Stefan.dimitrov@univ-grenoble-alpes.fr, hamiche@igbmc.fr

**Abstract**

H3.3 is a histone variant, which marks transcription start sites as well as telomeres and heterochromatic sites on the genome. H3.3 presence is thought to positively correlate with transcriptional status of its target genes. Using a conditional genetic strategy against H3.3B combined with short hairpin RNAs against H3.3A, we essentially depleted all H3.3 gene expression in mouse embryonic fibroblasts. Following nearly complete loss of H3.3 in cells, our transcriptomic analyses show very little impact on global gene expression as well as on histone variant H2A.Z localization. Instead, fibroblasts display slower cell growth and an increase in cell death coincident with large-scale chromosome misalignment in mitosis and large polylobed or micronuclei in interphase cells. Thus we conclude that H3.3 may additionally have an important under-explored role in chromosome segregation, nuclear structure and maintenance of genome integrity.

**Keywords**

H3.3, transcription, Mouse embryonic fibroblasts, RNA-seq, mitosis

**Introduction**

The replacement of canonical histones, core constituents of chromatin, by their variants drives chromatin dynamics and allows for functional and structural regulation of key cellular mechanisms (Boulard et al. 2007, Henikoff 2008). In contrast with replication dependent (RD) histones, the deposition of replication independent (RI) histones occurs in a cell cycle independent manner (Henikoff et al. 2004). There are RI variants for all the RD histones except for histone H4 (Hake et al. 2005, Pusarla and Bhargava 2005). The histone H3 variant H3.3 differs from its RD counterparts H3.1 and

H3.2 by only 5 or 4 amino-acids respectively (Szenker et al. 2011). Murine H3.3 is coded by two genes; *H3f3a* on chromosome 1 and *H3f3b* on chromosome 17, that despite variable mRNA sequences encode identical proteins (Krimer et al. 1993).

H3.3 containing nucleosomes, especially when associated with the histone H2A variant H2A.Z, may be promoting a less stable chromatin structure favorable to an active transcription state (Jin and Felsenfeld 2007, Jin et al. 2009). Accordingly, genome-wide localization studies have mapped H2A.Z and H3.3 at promoter regions and transcription start sites (TSS) and H3.3 density positively correlates with active transcription. However, H3.3 was also found associated with repressed genes and heterochromatic sites such as pericentric sites, telomeres and retroviral elements (Bargaje et al., 2012; Drané et al., 2010; Elsässer et al., 2015; Goldberg et al., 2010; Kraushaar et al., 2013). The differential deposition may reflect distinct targeting chaperone complexes. While the histone chaperone HIRA/ Ubinuclein (UBN1) targets H3.3 localization to TSS, the Death domain associated protein (DAXX) together with its chromatin remodeling partner Alpha Thalassemia/mental Retardation syndrome X-Linked (ATRX) are responsible for H3.3 deposition at pericentric heterochromatin and telomeres (Drané et al. 2010, Goldberg et al. 2010, Szenker et al. 2011, Daniel Ricketts et al. 2015).

Due to its presence at promoters and its higher enrichment at TSS and gene bodies of highly expressed genes (Goldberg et al. 2010), H3.3 has been strongly associated with a role in active transcription. It would thus be expected that transcription levels be highly impacted in the absence of H3.3. Intriguingly however, studies in the developing embryo showed that H3.3 depletion appears to have limited effect on gene transcription, while instead it seems to play an important role in the maintenance of genomic integrity (Bush et al. 2013, Jang et al. 2015). There is an increase in mitotic

defects and consequent aneuploidy as well as DNA damage in H3.3B knock-out mouse embryonic fibroblasts (MEF) (Bush et al. 2013) and H3.3 depleted embryonic stem cells (ESCs) (Banaszynski et al. 2013), indicative of chromosome structure dysfunction. Heterochromatin at telomeric, centromere, and pericentromeric repeat sequences presented a more open structure in the absence of H3.3 indicating a role for H3.3 in chromatin compaction (Jang et al. 2015).

Using a conditional gene-targeting strategy, we knocked out the histone *H3f3b* gene in MEFs and then using short hairpin RNAs against H3.3A mRNA in these cells, we derived cell lines that were essentially completely depleted of H3.3 expression. Deep RNA sequencing identified a set of nearly 800 genes that were mildly either up- or down-regulated in H3.3 depleted fibroblasts. Our results indicate that the loss of H3.3 has minimal impact on H2A.Z localization at the TSS and overall transcriptional rates. Importantly, H3.3 knockout cells display serious defects in mitotic progression including chromatin bridges in anaphase and misaligned chromosomes in metaphase and limits cell proliferation.

## Materials and methods

### Mouse strains

The FH-H3.3Bb mutant mouse line was established at the Phenomin-iCS (Phenomin - Institut Clinique de la Souris-, Illkirch, France; <http://www.ics-mci.fr/en/>). The targeting vector was constructed as follows. A 0.5 kb fragment encompassing exon 2 was amplified by PCR (from 129S2/SvPas ES cells genomic DNA) and subcloned in an iCS proprietary vector. This iCS vector contains a LoxP site as well as a floxed and flipped Neomycin resistance cassette. A DNA element encoding the FLAG-FLAG-HA epitope sequence was inserted in frame with the N-terminus of H3.3B. A 4.5 kb fragment

(corresponding to the 5' homology arm) and 3.5 kb fragment (corresponding to the 3' homology arms) were amplified by PCR and subcloned. The linearized construct was electroporated in 129S2/SvPas mouse embryonic stem (ES) cells. After selection, targeted clones were identified by PCR using external primers and further confirmed by Southern blot with 5' and 3' external probes. 2 positive ES clones were injected into C57BL/6N blastocysts, and the male chimaeras derived gave germline transmission. Mice were housed in the Plateforme de haute Technologie Animale (PHTA, Grenoble, France) mouse facility (agreement number C 38 516 10001, registered protocol n° 321 at ethical committee C2EA-12).

### Cell culture

Mouse embryonic fibroblasts (MEFs) were derived from E13.5 embryos. Heads and internal organs were removed and the torso was minced into chunks of tissue. Cells were cultured in DMEM high glucose, sodium pyruvate, Glutamax (Gibco) with 10% FBS and penicillin/streptomycin in a humidified incubator at 37°C and a 5% CO<sub>2</sub> atmosphere. Cells were maintained in culture using the 3T3 protocol (Xu 2005). *H3f3b*<sup>fl/fl</sup> MEFs were infected with adenovirus expressing Cre recombinase (Ad-CMV-iCre, Vector Biolabs, Philadelphia, PA) to disrupt the endogenous *H3f3b* allele. Virus was diluted in serum-free DMEM at a multiplicity of infection of 500. Infection medium was replaced with fresh complete medium the next day and cells were analyzed for knock-out efficiency after 3 days.

### Virus production and infections

293T cells were cotransfected with pLP1, pLP2, pLP3 and pLKO.1-shRNA vectors at a ratio of 1:0.5:0.6:2 respectively using Lipofectamine 2000 reagent (Invitrogen). shRNA

against H3.3A mRNA (Dharmacon GE, TRCN0000012026) to knock-down H3.3A or a scrambled control shRNA as control (shControl) was used. Transfection medium was replaced the next day with fresh complete medium. Viral supernatant was collected 48h post transfection and filtered through 0.45um filters. H3.3B KO MEFs at ~70% confluence were infected with the viral supernatant. Infection medium was replaced the next day and cells were selected with 3µg/ml puromycin. Cells were analyzed for knock-down efficiency 3 days later.

### qPCR

For gene expression analysis, total RNA was extracted with TRIzol (Life Technologies) and reverse-transcribed with Superscript II (Invitrogen) and random hexamer mix. Ribosomal protein S9 was used as the reference gene. Takara SYBR qPCR Premix Ex Taq (Tli RNaseH Plus) and LightCycler 480 (Roche) real-time system were used. qPCR cycling conditions were as follows: (3min 95°C [10s 95°C, 30s 60°C]x40).

The gene specific primers used were: Rps9\_F 5'TTGTCGCAAAACCTATGTGACC3',

Rps9\_R 5'GCCGCCTTACGGATCTTGG3', H3f3a\_F

5'ACAAAAGCCGCTCGCAAGAG3', H3f3a\_R 5'ATTTCTCGCACCAGACGCTG3',

H3f3b\_F 5'TGGCTCTGAGAGAGATCCGTCGTT, H3f3b\_R

5'GGATGTCTTTGGGCATGATGGTGAC3', Gadd45a\_F

5'TGCTGCTACTGGAGAACGAC3', Gadd45a\_R 5'TCCATGTAGCGACTTTCCCG3',

PDGFb\_F 5'GAGTCGGCATGAATCGCTG3', PDGFb\_R

5'GCCCCATCTTCATCTACGGA3', Edn1\_F 5'CCCACTCTTCTGACCCCTTT3',

Edn1\_R 5'GGCTCTGCACTCCATTCTCA3', Gas2\_F

5'GCCGAGATTTGGGAGTTGAT3', Gas2\_R 5'GCTTTATCAGACCAGGAGGC3',

Seh1l\_F 5'ATGACGGCTGTGTTAGGTTGT3', Seh1l\_R

5'TACTCAGCTGTGCTTTCTGCT3', Smad6\_F 5'GCCACTGGATCTGTCCGATT3',  
Smad6\_R 5'GGTCGTACACCGCATAGAGG3',

### Western blot

Cells were plated in 6-well plates and collected in 200µl of 2x Laemmli sample buffer (4% SDS, 20% Glycerol, 125mM Tris-HCl pH 6.8, 10% β-mercaptoethanol, 0.02% bromophenol blue). After brief sonication to fragment DNA, 20µl of sample was loaded and separated on 15% SDS-PAGE. Proteins were detected using anti-FLAG (1:2000, Sigma-Aldrich F3165) and anti-H4 (1:5000, Abcam ab10158)

### RNA-seq

After isolation of total cellular RNA from subconfluent MEFs using TRIzol reagent, libraries of template molecules suitable for strand specific high throughput DNA sequencing were created using “TruSeq Stranded Total RNA with Ribo-Zero Gold Prep Kit” (# RS-122-2301, Illumina). Briefly, starting with 300 ng of total RNA, the cytoplasmic and mitochondrial ribosomal RNA (rRNA) were removed using biotinylated, target-specific oligos combined with Ribo-Zero rRNA removal beads. Following purification, the RNA was fragmented into small pieces using divalent cations under elevated temperature. The cleaved RNA fragments were copied into first strand cDNA using reverse transcriptase and random primers, followed by second strand cDNA synthesis using DNA Polymerase I and RNase H. The double stranded cDNA fragments were blunted using T4 DNA polymerase, Klenow DNA polymerase and T4 PNK. A single 'A' nucleotide was added to the 3' ends of the blunt DNA fragments using a Klenow fragment (3' to 5' exo minus) enzyme. The cDNA fragments were ligated to double stranded adapters using T4 DNA Ligase. The ligated products were enriched by PCR

amplification (30s at 98°C; [10s at 98°C, 30s at 60°C, 30s at 72°C] x 12 cycles; 5min at 72°C). Then surplus PCR primers were removed by purification using AMPure XP beads (Agencourt Biosciences Corporation). Final cDNA libraries were checked for quality and quantified using 2100 Bioanalyzer (Agilent). The libraries were loaded in the flow cell at a concentration of 7pM, and clusters were generated in the Cbot and sequenced in the Illumina Hiseq 2500 as single-end 50 base reads following Illumina's instructions. Image analysis and base calling were performed using RTA 1.17.20 and CASAVA 1.8.2. Reads were mapped onto the mm9 assembly of the mouse genome by using Tophat (Trapnell et al. 2009) and the bowtie aligner (Langmead et al. 2009). Quantification of gene expression was performed using HTSeq (Anders et al. 2015) and gene annotations from Ensembl release 67. Read counts have been normalized across libraries with the statistical method proposed by Anders and Huber (Anders et al. 2010) and implemented in the DESeq Bioconductor library. Resulting p-values were adjusted for multiple testing by using the Benjamini and Hochberg method (Hochberg and Benjamin 1990).

The RNA-seq datasets (raw data as well as processed expression datasets) obtained in MEFs have been deposited in the Gene Expression Omnibus (GEO) under the accession number GSE84308.

### **Repeat analysis**

Repeat analyses of RNA-seq datasets were performed as follows. Reads were aligned to repetitive elements in two passes. In the first pass, reads were aligned to the non-masked mouse reference genome (NCBI37/mm9) using BWA v0.6.2 (Li and Durbin 2009). Positions of the reads uniquely mapped to the mouse genome were cross-

compared with the positions of the repeats extracted from UCSC (RMSK table in UCSC database for mouse genome mm9) and reads overlapping a repeat sequence were annotated with the repeat family. In the second pass, reads not mapped or multi-mapped to the mouse genome in the previous pass were aligned to RepBase v18.07 (Jurka et al. 2005) repeat sequences for rodent. Reads mapped to a unique repeat family were annotated with their corresponding family name. Finally, we summed up the read counts per repeat family of the two annotation steps. Data were normalized based upon library size. Difference of repeat read counts between samples was expressed as the  $\log_2$ -ratio (shH3.3A / shControl). The statistical significance of the difference between samples was assessed using the Bioconductor package DESeq. Processed datasets were restricted to repeat families with more than 100 mapped reads per RNA sample to avoid over- or underestimating fold enrichments due to low sequence representation.

### **Chromatin immunoprecipitation**

ChIP experiments were performed from 15 cm dishes of subconfluent MEFs.

For H2A.Z ChIP, cells were crosslinked with 1% paraformaldehyde for 7min at room temperature. The reaction was stopped by adding glycine to a final concentration of 0.125 M for 5 min. Input chromatin was diluted 1:10 for a final ChIP buffer composition of 20mM Tris, pH 8.0, 150mM NaCl, 2mM EDTA, 0.1% SDS, 1% Triton-X. 5  $\mu$ g of anti-IgG control (Abcam ab46540) or polyclonal anti-H2A.Z antibodies were added and incubated over-night on a rotary shaker at 4°C. A mix of 8 $\mu$ l of magnetic protein A and 8 $\mu$ l magnetic protein G beads (Dynabeads, Lifetechnology) were washed in ChIP buffer, resuspended in the original volume and added to the ChIP samples for 4-6 hours (rotary shaker, 4 °C). The magnetic beads were collected on a magnetic rack and washed for

5min with ChIP buffer, 5min with Wash buffer II (20mM Tris, pH 8.0, 500mM NaCl, 2mM EDTA, 0.1% SDS, 1% Triton-X) and 5min with Wash Buffer III (10mM Tris-HCl, pH 8.0, 1mM EDTA, 0.25M LiCl, 1% NP-40, 1% Sodium-deoxycholate (Na-DOC)). Immunoprecipitated material was eluted twice in 100µl of elution buffer (SDS 1%, 0.1 M NaHCO<sub>3</sub>) for 15 min at room temperature and crosslinks were reversed by incubating at 65 °C overnight.

For HA-H3.3 ChIP, 100µg of nuclei were digested with 2U of Micrococcal nuclease S7 (Roche 10107921001) in digestion buffer (10mM Tris-HCl, pH 7.5, 3mM CaCl<sub>2</sub>, 1x Protease inhibitors) for 12min at 37°C. 20µg of input chromatin was diluted in native chip buffer at a final concentration of 10mM Tris-HCl pH 7.5, 80mM NaCl, 1mM EDTA, 0.5% Triton-X. 20µl of anti-HA affinity matrix (Roche 118150160001) was added and incubated at 4°C overnight. Chromatin isolated from wild-type MEFs with no HA epitope was used as negative control. Beads-immunoprecipitated material were washed on rotary shaker with 10mM Tris-HCl pH 7.5, 80mM-150mM NaCl, 1mM EDTA, 0.5% Triton-X prior to elution and qPCR analysis.

Primers used for TSS analysis by qPCR were: Gadd45a-TSS\_F 5'TTTCCGCTCAACTCTGCCTT3', Gadd45a-TSS\_R 5'ACTCTGCACTGCTGCCTC3', Pdgfb-TSS\_F 5'AGCTCTGCGCTTTCTGATCT3', Pdgfb-TSS\_R 5'GATGGTTCGTCTTCACTCGC3', Edn1-TSS\_F 5'AACTAATCTGGTTCCTCCCGCC3', Edn1-TSS\_R 5'GAGGTGGGGCTGATCATTGT3', Gas2-TSS\_F 5'GTTACTAGAAAGCTCATGCCACT3', Gas2-TSS\_R 5'CCCAAACACTAAGCTAAGACAGA3', Seh1l-TSS\_F 5'TCATCACTGACTGCTGCTTC3', Seh1l-TSS\_R 5'CTTAGGAATGATGGGGACGC3', Smad6-TSS\_F 5'ATATCCTTCTGGGTCTTGCCA3', Smad6-TSS\_R 5'GCTCAAGGGTGTGTCAGCAAAA3'

### **Immunofluorescent staining**

Cells were fixed in formalin solution (Sigma-Aldrich) for 15min at 37°C, permeabilized with 0.2% Triton-X and incubated with lamin-B antibody (Santa-Cruz sc-6217) diluted 1/300 in 10% goat serum-PBS. Anti-goat IgG coupled with Cyanine 3 (Jackson 705-165-147) was used as secondary antibody. DNA was stained with the Hoechst 33342 (Invitrogen H3570) intercalating dye. All microscopy was performed on fixed cells with a Zeiss Axio Imager Z1 microscope with a Plan-Apochromat x63 objective. Z-stacks images were acquired with a Zeiss AxioCam camera piloted with the Zeiss Axiovision 4.8.10 software. All image treatment was performed using Fiji (ImageJ2-rc14) (Schindelin et al. 2012, 2015).

### **FACS analysis**

Cells were trypsinized and fixed in cold 70% ethanol overnight. After wash with PBS, cells were stained with propidium iodide (PI) solution containing 5µg/µl PI (Sigma Aldrich) and 200µg/mL RNase A at 37°C for 30minutes. Approximately 100,000 cells per condition were analyzed using Accuri C6 (Becton Dickinson). The percentage of cells in each phase of the cell cycle was determined using ModFit 4.1 software.

## **Results**

### **A combined genetic and shRNA strategy allows nearly complete depletion of H3.3 expression in mouse embryonic fibroblasts**

**Figure 1A** describes the strategy used to generate the transgenic knock-in epitope tagged 2XFLAG-HA-H3.3B (FH-H3.3B) mice line. Pregnant transgenic knock-in animals were sacrificed on day 13.5 post fertilization and isolated embryos were used to derive

mouse embryonic fibroblasts (MEFs) using the 3T3 protocol (Xu 2005) (**Figure 1B**). Cells were treated with a Cre expressing adenovirus to generate H3.3B knockout (KO) cells in culture. Single cells were selected and clonally expanded and genotyped to confirm the deletion of the *H3f3b* gene. Loss of H3.3B expression was verified by qPCR as well as by immunoblotting for the Flag epitope (**Figures 1C, 1D**). H3.3B KO MEFs were then subsequently stably transfected with a scrambled control shRNA (shControl) or an shRNA targeting the coding sequence of H3.3A mRNA (shH3.3A). H3.3B knockout (H3.3B KO) cells transduced with control shRNA (shControl) displayed a fold increase in H3.3A mRNA levels while cells treated with shRNA against H3.3A (shH3.3A) showed a near complete knockdown (Kd) of H3.3A mRNA expression (**Figure 1C**). All cells displayed fibroblast like behavior and H3.3 depleted cell lines (H3.3B KO / H3.3A Kd) were slower to grow in culture as shown by the increase in their doubling time (**Figure 1E**).

### H3.3 depletion has a mild effect on the global transcriptome

We then isolated total RNA from control shRNA treated H3.3B KO cells and from H3.3B KO / H3.3A Kd MEFs and carried out Ribozero RNA-seq analysis. RNA-seq analysis was carried out on pooled datasets from biological duplicate experiments. As seen in qPCR experiments (**Figure 1C**), H3.3A expression was significantly reduced in the H3.3B KO / H3.3A Kd MEFs cells (**Figure 2A**). A large fraction of the expressed genome does not change at the transcriptomic level in H3.3 depleted cells. Around 4% of transcribed genes in MEFs (800 genes in total) are mildly misregulated in H3.3 depleted cells with ~400 of them displaying upregulated expression and another 400 with downregulated expression with respect to the control cells ( $P < 0.05$  cutoff) (**Figure 2B**).

H3.3 was recently implicated in maintenance of the silent state of endogenous retroviruses (ERVs) in the mouse genome (Elsässer et al. 2015). However, no significant changes could be seen in the global transcription of DNA repeats such as retro-elements (including long terminal repeats (LTR), ERV, long (LINE) and short (SINE) interspersed nuclear elements) or tandem repeats (including major satellites, telomeres and microsatellites), which account for more than 40% of the mouse genome (**Figure 2C**). Functional clustering of differentially expressed genes indicated significant downregulation of genes implicated in lipid and sterol processing while factors involved in cell adhesion and motility were upregulated (**Figure 2D**). There was also dysregulation in the expression of genes involved in cell cycle progression (**Figure 2E**). We compared our gene expression profile to that of the H3.3 null embryos in a *p53*-null background (Jang et al. 2015) and to H3.3B KO/H3.3A Kd ESCs (Banaszynski et al. 2013). Even though all three studies indicate very little impact on global transcription, an overlap between the datasets was essentially non-existent and limited to 9 genes in comparison to H3.3 depleted embryos and 6 genes in comparison to H3.3 depleted ESCs (**Figure 2F**).

### **H2A.Z variant dynamics are not affected at differentially expressed genes in H3.3 depleted cells**

We then selected 6 genes that were either up- or down-regulated in H3.3B-KO compared to H3.3B KO / H3.3A Kd fibroblasts and validated their gene expression levels by RT-qPCR analysis (**Figure 3A**). While the change in gene expression was about 50% for the selected genes (as seen in the RNA-seq analysis), with the exception of *Gadd45a* which was upregulated nearly 7 times, most other genes (*Pdgfb*, *Edn1*)

showed a change in expression of 2-3 fold. To determine the extent to which H3.3 is present at the transcription start sites (TSS) of these 6 candidate genes, we isolated chromatin from FH-H3.3B MEFs and performed native chromatin immunoprecipitation (ChIP) experiments using an antibody against the HA tag. ChIP on isolated mononucleosomes indicated that H3.3 was highly enriched relative to input DNA at all of the selected candidate TSS regions (**Figure 3B**). Mononucleosomes from wild-type mouse fibroblasts, used as a control for ChIP to rule out non-specific interaction with the antibody, showed essentially no enrichment at the TSS. Thus, while the presence of H3.3 at the transcription start sites is thought to positively correlate with transcription, its depletion from cells has a muted impact on overall transcription rates.

Histone variant H2A.Z also marks the TSS of genes and the presence of dual H3.3-H2A.Z variant nucleosomes is thought to positively regulate inducible transcription (Jin and Felsenfeld 2007, Henikoff 2008, Jin et al. 2009, Obri et al. 2014). We then tested if the deposition of the histone variant H2A.Z at the TSS of these selected candidate genes was affected by the depletion of H3.3 from the fibroblasts. Crosslinked and sonicated chromatin was generated from either WT, H3.3B KO cells or from H3.3 depleted (H3.3B KO / H3.3A Kd) cells and H2A.Z deposition was determined relative to a control IgG (**Figure 3C**). At all the TSS examined, loss of H3.3 did not have a significant impact on H2A.Z deposition regardless of the transcriptional changes of the corresponding genes.

### **H3.3 depletion results in defective mitotic progression**

Following the shRNA mediated depletion of H3.3A and in stark comparison to control cells, we observed an increase in the rate of cell doubling time in culture as well as increased rate of cell death. Depletion of H3.3 from fibroblasts resulted in cells with

larger nuclei, increased number of micronuclei and polylobed nuclear structures in interphase cells (**Figures 4A and 4B**). Loss of H3.3B alone led to a doubling of the number of interphase nuclear defects while complete depletion of H3.3 led to a near 3 time increase of polylobed and micronuclei appearance (**Figure 4C**). While there was nearly a 50% reduction in the number of cells entering mitosis in H3.3 depleted fibroblasts, in addition, these cells displayed marked defects in chromosome alignment at the metaphase plate, lagging chromosomes in anaphase as well as telophase bridges, indicating chromosome structure dysregulation (**Figures 4B, 4D and 4E**). Finally, FACS analyses indicated that as compared to wild-type or control FH-H3.3B cells, H3.3B KO and H3.3A Kd/H3.3B KO depleted cells showed progressively increased residence time in G0/G1 phase of the cell cycle and relatively fewer cells in S-phase or mitosis (**Figure 4E**).

### Discussion and conclusion

Recent research by Jang et al. on H3.3 function in the developing embryo have surprisingly shown that the loss of H3.3 function has very little impact on global transcription, with most affected genes being up- or downregulated by not much greater than 2-fold (Jang et al. 2015). In this study, we extend our analysis to mouse embryonic fibroblasts and intriguingly observe very similar results to the study by Jang et al.- *i.e.* little to no effect on global transcription. Using a novel transgenic 'conditional knock-in/knockout' mouse model for H3.3B, we generated mouse fibroblasts that yielded H3.3B knockout cells upon Cre expression. Further expression of a specific and efficient shRNA against H3.3A resulted in almost complete depletion of H3.3 expression from fibroblasts. We then performed genome-wide transcriptome analysis and found very few genes (~4% of transcribed genes) showing significant changes in gene expression.

While this result is similar to what was described in embryos, the ensemble of the affected transcriptome shows little to no overlap between the two experimental studies. Furthermore, our results suggest that the changes at the transcriptional level in H3.3 knockout cells do not impact histone variant H2A.Z presence at the TSS of the selected genes. Thus, despite the positive correlation between the transcriptional rate of genes and H3.3 accumulation at their corresponding TSS, the global effect on transcription observed upon H3.3 depletion is suggestive of a facilitative role rather than that of an essential positive regulatory factor. This also correlates with what has been observed in the past in mouse embryos as well as stem cells (Wong et al. 2010, Banaszynski et al. 2013, Jang et al. 2015). Recent data has demonstrated a silencing role for H3.3 by localization at endogenous retroviral elements (ERVs) in ESCs (Elsässer et al. 2015). Our study has not revealed an impact on ERV transcription upon H3.3 depletion in MEFs. The role of H3.3 in retrotransposon silencing may therefore be specific to pluripotent cells and replaced by other mechanisms during differentiation.

Thus, our study supports an understudied key role of H3.3 in maintenance of genome integrity. H3.3 knockout ES cells and mouse fibroblasts show dramatic defects in mitosis with 3-4 times increase in the number of defects such as lagging chromosomes, anaphase bridges while the total number of cells entering mitosis is much lower in H3.3 null cells. We also observed significant changes to the nuclear matrix structure in interphase cells with the appearance of many polylobed and micronuclei in H3.3 depleted cells. Unlike Jang et al, wherein the impact of H3.3 loss was studied in a p53 null background, our cells are completely depleted for H3.3B and H3.3A is knocked-down with greater than 90% efficiency. However, the similarity of the results indicates a key role for H3.3 in regulating faithful chromosome segregation during mitosis and perhaps in maintaining nuclear architecture in interphase.

In conclusion, we depleted H3.3 expression in mouse embryonic fibroblasts combining genetic and shRNA strategies. This near complete depletion of H3.3 from mammalian fibroblasts affected transcription at a handful of genes, while global transcription rates were altered only about 2-fold with no effect seen at all on expression of retroviral repeat elements. Instead, we showed that H3.3 plays an important role in faithful completion of the cellular mitotic program and maintaining genomic integrity.

### Abbreviations

**TSS:** transcription start sites **MEF:** mouse embryonic fibroblasts **ESC:** embryonic stem cells **KO:** knock-out **Kd:** knock-down **ERV:** endogenous retroviral elements **LTR:** long terminal repeats **LINE and SINE:** long and short interspersed nuclear element **RNA-seq:** ribonucleic acid sequencing **RT-qPCR:** reverse transcription quantitative polymerase chain reaction **rRNA:** ribosomal RNA **s.e.m.:** standard error of the mean **PI:** propidium iodide **WT:** wild-type

### Acknowledgements

This work was supported by institutional funds from the Université de Strasbourg-UDS, the Université de Grenoble Alpes-UGA, the Centre National de la Recherche Scientifique-CNRS, the Institut National de la Santé et de la Recherche Médicale-INSERM (Plan Cancer), and by grants from : the ATIP AVENIR program (K.P.), the Institut National du Cancer-INCA (INCa\_4496, INCa\_4454 and INCa PLBIO15-245), the Fondation pour la Recherche Médicale-FRM (DEP20131128521), the Université de Strasbourg Institut d'Etudes Avancées (USIAS-2015-42) (A.H), the Association pour la Recherche sur le Cancer, La Ligue Nationale contre le Cancer (Équipe labellisée to

A.H). A.O. was awarded the European Molecular Biology Organization (EMBO) short-term fellowship, Scientific and Technological Research Council of Turkey (TUBITAK) 2214/A doctoral research grant and French Ministry of Foreign Affairs scholarship. Sequencing was performed by the IGBMC Microarray and Sequencing platform, a member of the 'France Génomique' consortium (ANR-10-INBS-0009).

## References

Anders, S., Huber, W., Nagalakshmi, U., Wang, Z., Waern, K., Shou, C., Raha, D., Gerstein, M., Snyder, M., Mortazavi, A., Williams, B., McCue, K., Schaeffer, L., Wold, B., Robertson, G., Hirst, M., Bainbridge, M., Bilenky, M., Zhao, Y., Zeng, T., Euskirchen, G., Bernier, B., Varhol, R., Delaney, A., Thiessen, N., Griffith, O., He, A., Marra, M., Snyder, M., Jones, S., Licatalosi, D., Mele, A., Fak, J., Ule, J., Kayikci, M., Chi, S., Clark, T., Schweitzer, A., Blume, J., Wang, X., Darnell, J., Darnell, R., Smith, A., Heisler, L., Mellor, J., Kaper, F., Thompson, M., Chee, M., Roth, F., Giaever, G., Nislow, C., Marioni, J., Mason, C., Mane, S., Stephens, M., Gilad, Y., Wang, L., Feng, Z., Wang, X., Wang, X., Zhang, X., Robinson, M., Smyth, G., Whitaker, L., Robinson, M., McCarthy, D., Smyth, G., Robinson, M., Smyth, G., Cameron, A., Trivedi, P., Robinson, M., Oshlack, A., Loader, C., McCullagh, P., Nelder, J., Agresti, A., Engström, P., Tommei, D., Stricker, S., Smith, A., Pollard, S., Bertone, P., Morrissy, A., Morin, R., Delaney, A., Zeng, T., McDonald, H., Jones, S., Zhao, Y., Hirst, M., Marra, M., Kasowski, M., Grubert, F., Heffelfinger, C., Hariharan, M., Asabere, A., Waszak, S., Habegger, L., Rozowsky, J., Shi, M., Urban, A., Hong, M., Karczewski, K., Huber, W., Weissman, S., Gerstein, M., Korbil, J., Snyder, M., Benjamini, Y., Hochberg, Y., Bullard, J., Purdom, E., Hansen, K., Dudoit, S., Bloom, J., Khan, Z., Kruglyak, L., Singh, M.,

- Caudy, A., Smyth, G., Smyth, G., Lönnstedt, I., Speed, T., Gentleman, R., Carey, V., Bates, D., Bolstad, B., Dettling, M., Dudoit, S., Ellis, B., Gautier, L., Ge, Y., Gentry, J., Hornik, K., Hothorn, T., Huber, W., Iacus, S., Irizarry, R., Leisch, F., Li, C., Maechler, M., Rossini, A., Sawitzki, G., Smith, C., Smyth, G., Tierney, L., Yang, J., Zhang, J., Bliss, C., Fisher, R., Clark, S., Perry, J., Lawless, J., Saha, K., Paul, S., Langmead, B., Trapnell, C., Pop, M., and Salzberg, S. 2010. Differential expression analysis for sequence count data. *Genome Biol.* **11**(10): R106. doi:10.1186/gb-2010-11-10-r106.
- Anders, S., Pyl, P.T., and Huber, W. 2015. HTSeq-A Python framework to work with high-throughput sequencing data. *Bioinformatics* **31**(2): 166–169. doi:10.1093/bioinformatics/btu638.
- Banaszynski, L.A., Wen, D., Dewell, S., Whitcomb, S.J., Lin, M., Diaz, N., Chappier, A., Goldberg, A.D., Canaani, E., Rafii, S., Zheng, D., Elsa, S.J., and Allis, C.D. 2013. Facilitates PRC2 Recruitment at Developmental Loci in ES Cells. **5**: 107–120. doi:10.1016/j.cell.2013.08.061.
- Bargaje, R., Alam, M.P., Patowary, A., Sarkar, M., Ali, T., Gupta, S., Garg, M., Singh, M., Purkanti, R., Scaria, V., Sivasubbu, S., Brahmachari, V., and Beena Pillai. 2012. Proximity of H2A.Z containing nucleosome to the transcription start site influences gene expression levels in the mammalian liver and brain. *Nucleic Acids Res.* **40**(18): 8965–8978. doi:10.1093/nar/gks665.
- Boulard, M., Bouvet, P., Kundu, T.K., and Dimitrov, S. 2007. No TitleHistone variant nucleosomes: structure, function and implication in disease. *Subcell. Biochem.* **41**: 71–89.
- Bush, K.M., Yuen, B.T., Barrilleaux, B.L., Riggs, J.W., O'Geen, H., Cotterman, R.F., and Knoepfler, P.S. 2013. Endogenous mammalian histone H3.3 exhibits chromatin-

related functions during development. *Epigenetics Chromatin* **6**(1): 7.

doi:10.1186/1756-8935-6-7.

Daniel Ricketts, M., Frederick, B., Hoff, H., Tang, Y., Schultz, D.C., Singh Rai, T., Grazia Vizioli, M., Adams, P.D., and Marmorstein, R. 2015. Ubinuclein-1 confers histone H3.3-specific-binding by the HIRA histone chaperone complex. *Nat. Commun.* **6**: 7711. doi:10.1038/ncomms8711.

Dran??, P., Ouararhni, K., Depaux, A., Shuaib, M., and Hamiche, A. 2010. The death-associated protein DAXX is a novel histone chaperone involved in the replication-independent deposition of H3.3. *Genes Dev.* **24**(12): 1253–1265.

doi:10.1101/gad.566910.

Elsässer, S.J., Noh, K.-M., Diaz, N., Allis, C.D., and Banaszynski, L.A. 2015. Histone H3.3 is required for endogenous retroviral element silencing in embryonic stem cells. *Nature* **522**(7555): 240–4. doi:10.1038/nature14345.

Goldberg, A.D., Banaszynski, L.A., Noh, K.M., Lewis, P.W., Elsaesser, S.J., Stadler, S., Dewell, S., Law, M., Guo, X., Li, X., Wen, D., Chapgier, A., DeKever, R.C., Miller, J.C., Lee, Y.L., Boydston, E.A., Holmes, M.C., Gregory, P.D., Grealley, J.M., Rafii, S., Yang, C., Scambler, P.J., Garrick, D., Gibbons, R.J., Higgs, D.R., Cristea, I.M., Urnov, F.D., Zheng, D., and Allis, C.D. 2010. Distinct Factors Control Histone Variant H3.3 Localization at Specific Genomic Regions. *Cell* **140**(5): 678–691. Elsevier Ltd. doi:10.1016/j.cell.2010.01.003.

Hake, S.B., Garcia, B. a, Kauer, M., Baker, S.P., Shabanowitz, J., Hunt, D.F., and Allis, C.D. 2005. Serine 31 phosphorylation of histone variant H3.3 is specific to regions bordering centromeres in metaphase chromosomes. *Proc. Natl. Acad. Sci. U. S. A.* **102**(18): 6344–6349. doi:10.1073/pnas.0502413102.

Henikoff, S. 2008. Nucleosome destabilization in the epigenetic regulation of gene

- expression. *Nat Rev Genet* **9**(1): 15–26. doi:nrg2206 [pii]\n10.1038/nrg2206.
- Henikoff, S., Furuyama, T., and Ahmad, K. 2004. Histone variants, nucleosome assembly and epigenetic inheritance. *Trends Genet.* **20**(7): 320–326. doi:10.1016/j.tig.2004.05.004.
- Hochberg, Y., and Benjamin, Y. 1990. More Powerful Procedures for Multiple Significance Testing. **9**(July 1988): 811–818.
- Jang, C., Shibata, Y., Starmer, J., Yee, D., and Magnuson, T. 2015. Histone H3 . 3 maintains genome integrity during mammalian development. *Genes Dev.* **1**: 1377–1392. doi:10.1101/gad.264150.115.GENES.
- Jin, C., and Felsenfeld, G. 2007. Nucleosome stability mediated by histone variants H3.3 and H2A.Z. *Genes Dev.* **21**(12): 1519–1529. doi:10.1101/gad.1547707.
- Jin, C., Zang, C., Wei, G., Cui, K., Peng, W., Zhao, K., and Felsenfeld, G. 2009. H3.3/H2A.Z double variant-containing nucleosomes mark “nucleosome-free regions” of active promoters and other regulatory regions. *Nat. Genet.* **41**(8): 941–5. Nature Publishing Group. doi:10.1038/ng.409.
- Jurka, J., Kapitonov, V. V., Pavlicek, A., Klonowski, P., Kohany, O., and Walichewicz, J. 2005. Repbase Update, a database of eukaryotic repetitive elements. *Cytogenet. Genome Res.* **110**(1–4): 462–467. doi:10.1159/000084979.
- Kraushaar, D.C., Jin, W., Maunakea, A., Abraham, B., Ha, M., and Zhao, K. 2013. Genome-wide incorporation dynamics reveal distinct categories of turnover for the histone variant H3.3. *Genome Biol.* **14**(10): R121. doi:10.1186/gb-2013-14-10-r121.
- Krimer, D.B., Cheng, G., and Skoultchi, A.I. 1993. Induction of H3.3 replacement histone mRNAs during the precommitment period of murine erythroleukemia cell differentiation. *Nucleic Acids Res* **21**(12): 2873–2879. doi:10.1093/nar/21.12.2873.
- Langmead, B., Trapnell, C., Pop, M., and Salzberg, S. 2009. Ultrafast and memory-

- efficient alignment of short DNA sequences to the human genome. *Genome Biol.* **10**(3): R25. doi:10.1186/gb-2009-10-3-r25.
- Li, H., and Durbin, R. 2009. Fast and accurate short read alignment with Burrows-Wheeler transform. *Bioinformatics* **25**(14): 1754–1760. doi:10.1093/bioinformatics/btp324.
- Obri, A., Ouararhni, K., Papin, C., Diebold, M.-L., Padmanabhan, K., Marek, M., Stoll, I., Roy, L., Reilly, P.T., Mak, T.W., Dimitrov, S., Romier, C., and Hamiche, A. 2014. ANP32E is a histone chaperone that removes H2A.Z from chromatin. *Nature* **505**(7485): 648–53. Nature Publishing Group. doi:10.1038/nature12922.
- Pusarla, R.H., and Bhargava, P. 2005. Histones in functional diversification: Core histone variants. *FEBS J.* **272**(20): 5149–5168. doi:10.1111/j.1742-4658.2005.04930.x.
- Schindelin, J., Arganda-Carreras, I., Frise, E., Kaynig, V., Longair, M., Pietzsch, T., Preibisch, S., Rueden, C., Saalfeld, S., Schmid, B., Tinevez, J.-Y., White, D.J., Hartenstein, V., Eliceiri, K., Tomancak, P., and Cardona, A. 2012. Fiji: an open-source platform for biological-image analysis. *Nat Meth* **9**(7): 676–682. Nature Publishing Group, a division of Macmillan Publishers Limited. All Rights Reserved. Available from <http://dx.doi.org/10.1038/nmeth.2019>.
- Schindelin, J., Rueden, C.T., Hiner, M.C., and Eliceiri, K.W. 2015. The ImageJ ecosystem: An open platform for biomedical image analysis. *Mol. Reprod. Dev.* **82**(7–8): 518–529. doi:10.1002/mrd.22489.
- Szenker, E., Ray-Gallet, D., and Almouzni, G. 2011. The double face of the histone variant H3.3. *Cell Res* **21**(3): 421–434. Nature Publishing Group. doi:10.1038/cr.2011.14.
- Trapnell, C., Pachter, L., and Salzberg, S.L. 2009. TopHat: Discovering splice junctions

with RNA-Seq. *Bioinformatics* **25**(9): 1105–1111.

doi:10.1093/bioinformatics/btp120.

Wong, L.H., Mcghee, J.D., Sim, M., Anderson, M.A., Ahn, S., Hannan, R.D., George, A.J., Morgan, K.A., Mann, J.R., and Choo, K.H.A. 2010. ATRX interacts with H3 . 3 in maintaining telomere structural integrity in pluripotent embryonic stem cells. : 351–360. doi:10.1101/gr.101477.109.20.

Xu, J. 2005. Preparation, Culture, and Immortalization of Mouse Embryonic Fibroblasts. *Curr. Protoc. Mol. Biol.* **Chapter 28**: 1–8. doi:10.1002/0471142727.mb2801s70.

## Figure Legends

### Figure 1. Generation of H3.3 MEF models and H3.3 expression.

**A.** (i) Wild-type *H3f3b* gene structure. The open reading frame is indicated by black boxes (ii) A DNA element encoding the FLAG-FLAG-HA amino acids was inserted in frame with the N-terminus of H3.3B. In addition, a loxP site was inserted on both ends of Exon 2. A mouse line was derived from ES cells carrying the modified *H3f3b<sup>fl/fl</sup>* allele (iii) Structure of the H3.3B KO, after Cre recombinase expression, which deletes exon 2 and generates loss of function (KO) allele, *H3f3b<sup>-/-</sup>*. **B.** FH-H3.3B Mouse embryonic fibroblasts (MEFs) isolated from *H3f3b<sup>fl/fl</sup>* embryos at 13.5 dpf. Immortalized MEFs were infected with Cre recombinase expressing adenovirus to generate loss of function allele. *H3f3b<sup>-/-</sup>* MEFs were further infected with either a scrambled control shRNA (shControl) or one targeting the H3.3A mRNA (shH3.3A) to produce H3.3B knockout (KO) / H3.3A Knockdown (Kd) MEFs. **C.** Relative H3.3 RNA expression in MEFs. Quantitative RT-qPCR mRNA profiles normalized to ribosomal protein S9 (Rps9) mRNA and relative to the values obtained for the control FH-H3.3B MEFs set at  $1.0 \pm \text{s.e.m.}$  One-way ANOVA,  $P < 0.001$  for FH-H3.3B vs H3.3B KO and  $P < 0.01$  for FH-H3.3B vs. H3.3B

KO / H3.3A Kd, n=4. **D.** Western blot analysis of the loss of FH-H3.3B expression after Cre expression. **E.** Average doubling times in MEFs. 25,000 cells of each cell type were plated and counted at different times to calculate the doubling time. Error bars represent standard deviation, one-way ANOVA,  $P < 0.001$  for FH-H3.3B vs. H3.3B KO / H3.3A Kd, n=4.

**Figure 2. Genome-wide transcriptome analysis of MEFs in the absence of H3.3.**

**A.** Bar graph representing H3.3A expression in control H3.3BKO and H3.3A Kd/H3.3B KO / H3.3A Kd MEFs. **B.** Scatter plots comparing gene expression profiles of control (shControl) and H3.3B KO / H3.3A Kd (shH3.3A) MEFs. Red dots indicate differentially expressed genes ( $P < 0.05$  and  $|\log_2 \text{fc}| > 1$ ). **C.** Scatter plots comparing global transcription of repeat families in H3.3B KO and H3.3B KO / H3.3A Kd MEFs. **D.** Functional annotation clustering of differentially expressed genes. **E.** List of the differentially expressed genes implicated in mitosis. **F.** Comparative analysis of the differentially expressed genes in H3.3 deficient embryos (Jang et al. 2015) and in H3.3 depleted ESCs (Banaszynski et al. 2013). Lists of genes that show similar patterns of up or downregulation in transcription are indicated.

**Figure 3. H3.3 and H2A.Z enrichment at transcription start sites (TSS) of genes showing differential mRNA expression.**

**A.** Quantitative PCR assay for gene expression in H3.3B KO and H3.3B KO / H3.3A Kd MEFs. RNA values are normalized to ribosomal protein S9 (Rps9) mRNA and are relative to H3.3B KO value set at  $1.0 \pm \text{s.e.m.}$ , two-tailed t-test,  $P < 0.05$  for *Sehl1*,  $P < 0.01$  for *Gadd45a*, *Pdgfb*, *Gas2*, *Smad 6*,  $P < 0.001$  for *Edn1*, n=4 **B.** H3.3B enrichment at TSS of differentially transcribed genes by ChIP-quantitative PCR assay (ChIP-

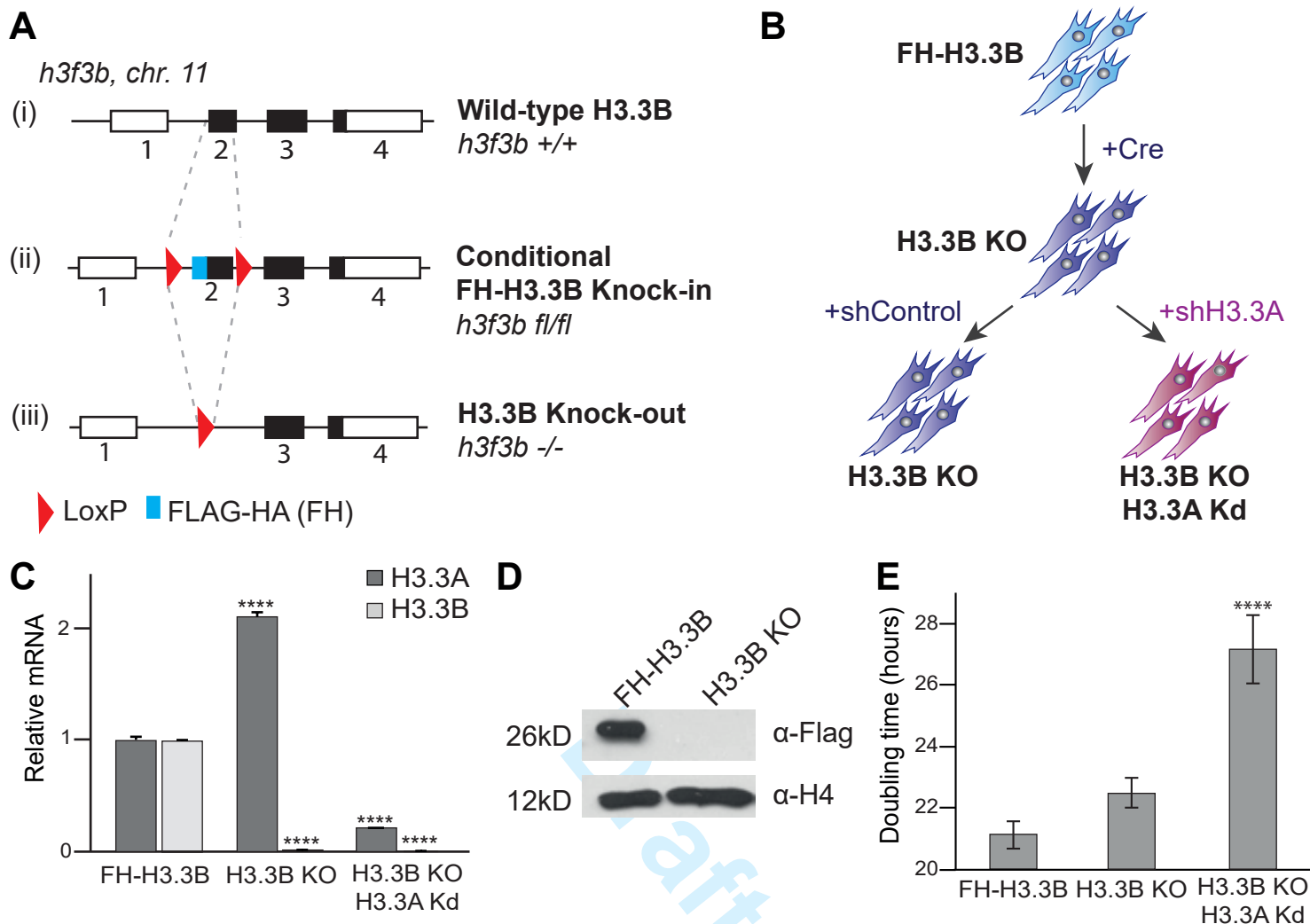
qPCR). Values are expressed in % of enrichment relative to input  $\pm$  s.e.m. Chromatin from wild-type (WT) MEFs containing no HA-tag were used as a negative IP control. The TSS of examined genes were significantly enriched in H3.3B compared to the negative control, one-tailed t-test,  $n=4$ ,  $P < 0.01$  for *Pdgfb* and *Smad6*,  $P < 0.001$  for *Edn1* and *Seh1l*, and  $P < 0.0001$  for *Gadd45a* and *Gas2*. **C.** H2A.Z enrichment at TSS of differentially transcribed genes. ChIP-qPCR assay. Values are expressed in enrichment relative to input  $\pm$  s.e.m. Rabbit IgG was used as the control. The TSS of examined genes were significantly enriched in H2A.Z compared to the negative control, one-tailed t-test,  $P < 0.05$ ,  $n=3$ . ChIP-qPCR graphs are representative of 3 separate experiments. H2A.Z enrichment at studied TSS did not vary significantly between samples (One-way ANOVA test,  $P > 0.05$ ,  $n=3$ ).

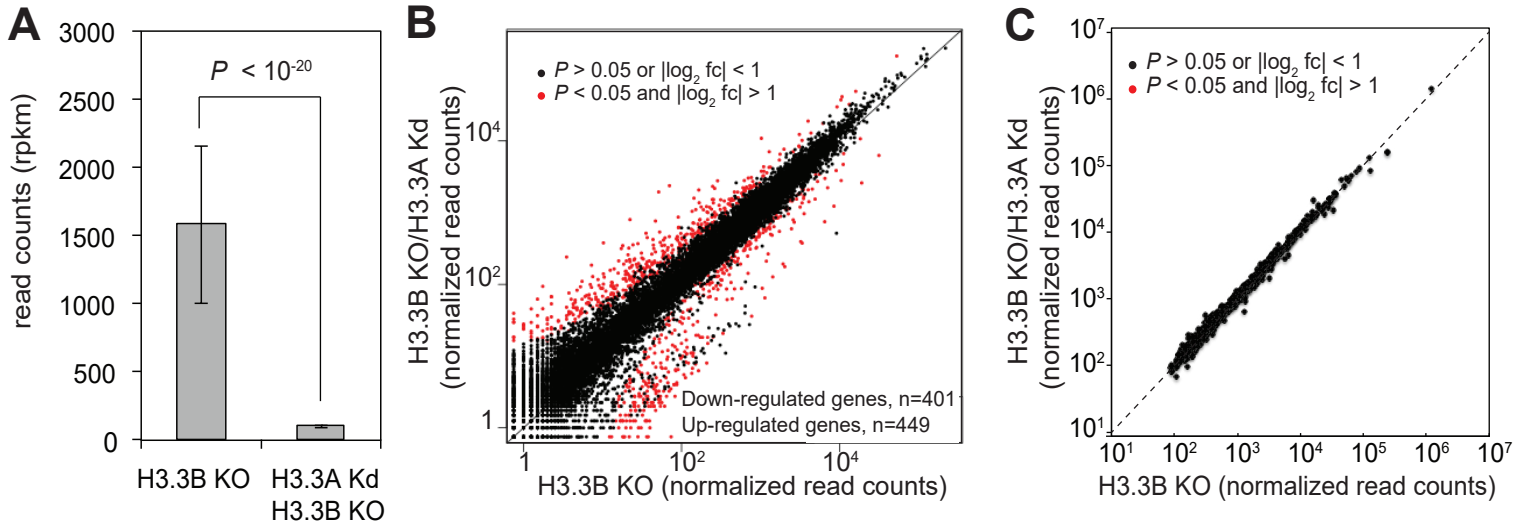
#### **Figure 4. Mitotic defects in H3.3 deficient MEFs.**

**A.** Representative images of control nuclei. **B.** Representative image of nuclear abnormalities with micronuclei and polylobed nuclei and of mitotic abnormalities with chromatin bridges, misaligned and lagging chromosomes observed in H3.3 deficient MEFs. Defects are indicated by yellow arrows. **C.** Nuclear abnormalities in control FH-H3.3B and H3.3 deficient MEFs. One-way ANOVA,  $P < 0.05$  for FH-H3.3B vs. H3.3B KO and  $P < 0.001$  for FH-H3.3B vs. H3.3B KO / H3.3A Kd MEFs,  $n=4$ . **D.** Mitotic abnormalities in control FH-H3.3B and H3.3 deficient MEFs. 125 mitotic events were scored for each line and experiment. Error bars represent the standard deviation between experiments on the total number of abnormalities. One-way ANOVA  $P < 0.01$  for FH-H3.3B vs. H3.3B KO and  $P < 0.0001$  for FH-H3.3B vs. H3.3B KO / H3.3A Kd MEFs,  $n=3$ . **E.** Flow cytometric analysis of cell cycle for wild-type (WT), FH-H3.3B, H3.3B KO and double H3.3B KO / H3.3A Kd cells treated with propidium iodide (PI).

Approximately 100,000 cells per condition were analyzed per experiment. Error bars represent the standard deviation between experiments (One-way ANOVA,  $P < 0.01$  for WT vs. H3.3B KO / H3.3A Kd,  $n=3$ ).

Draft





**D**

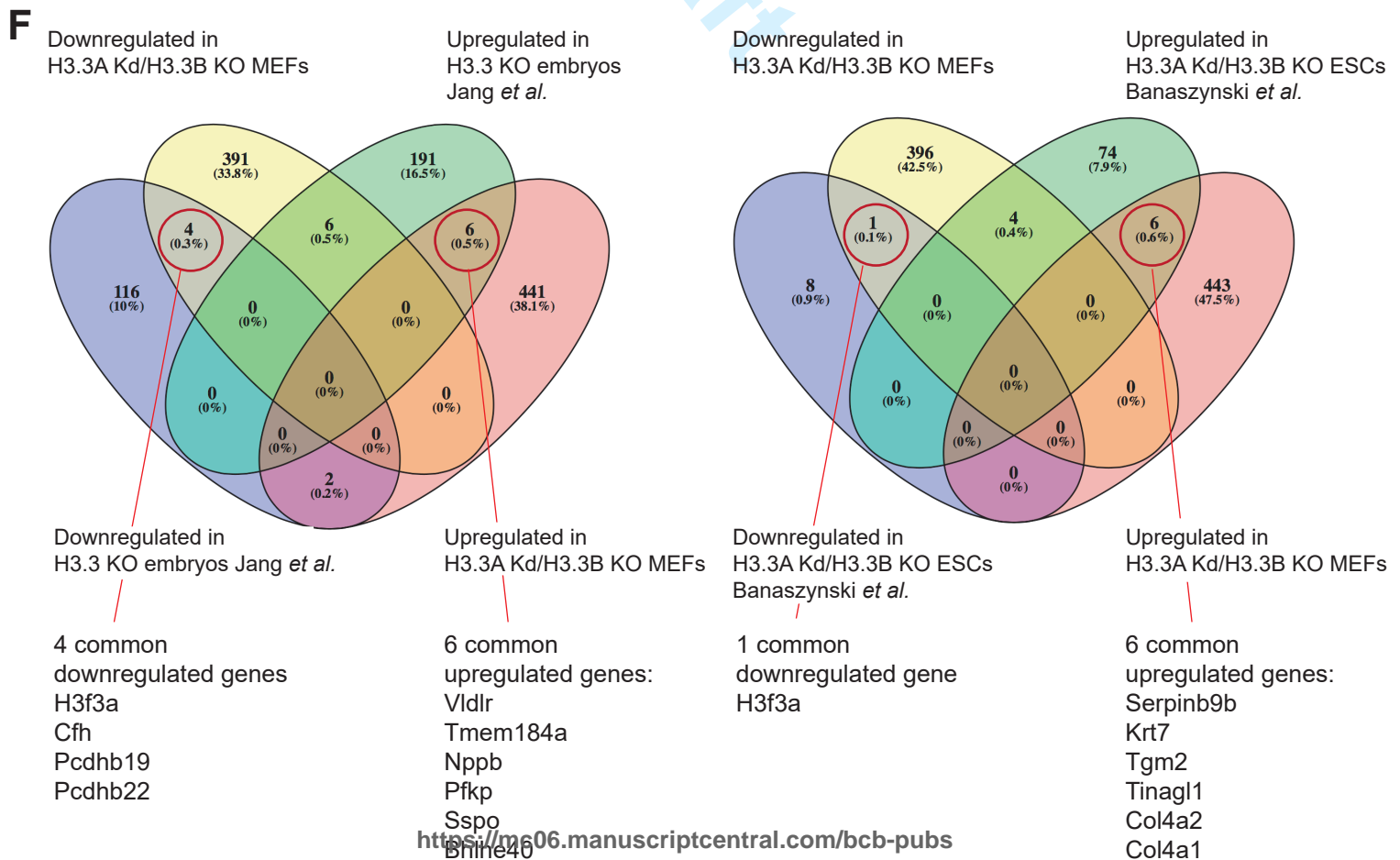
Annotation cluster	Enrichment score	P value
Secreted/glycoprotein	17.57	1,10E-22
Microsome	10.41	3,90E-16
Polysaccharide binding	6.94	1,80E-06
Complement / immune response	6.56	1,50E-16
Steroid metabolic process	4.94	8,40E-05
High-density lipoprotein	4.9	2,00E-08
Secreted/glycoprotein	8.5	1,40E-08
Contractile fiber	8.37	1,50E-08
Cell adhesion	7.47	9,60E-06

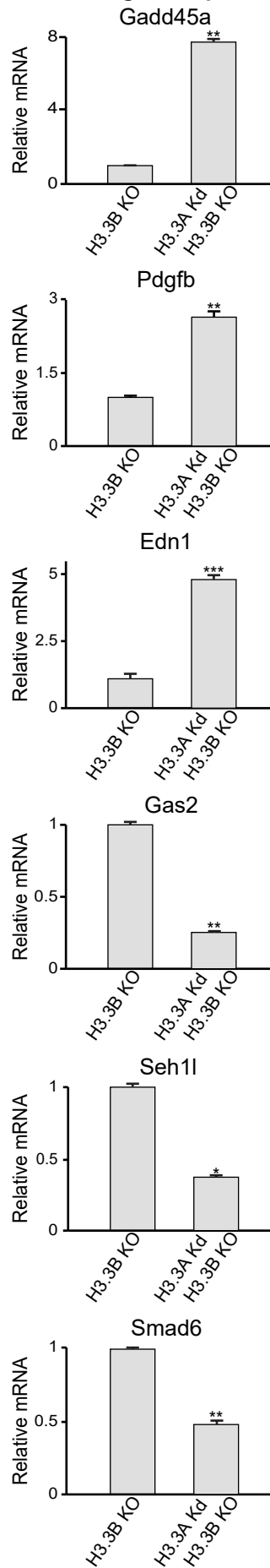
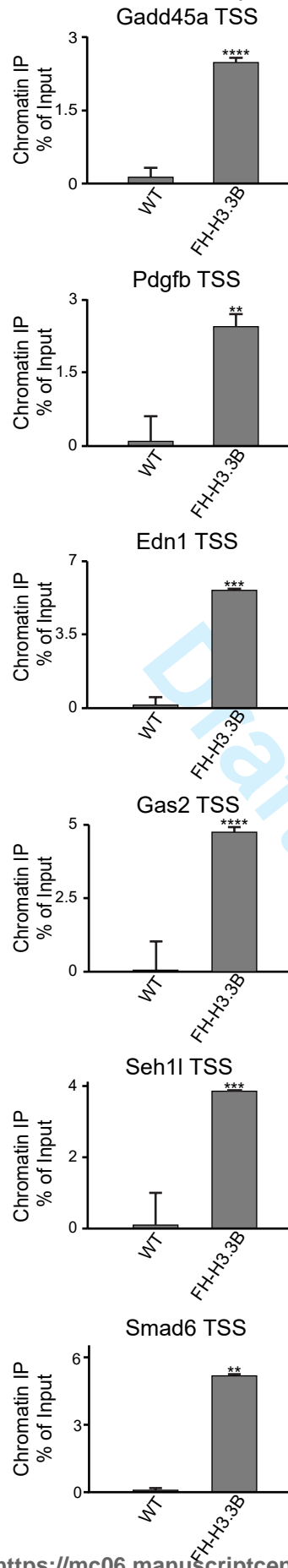
**Down**

**Up**

**E**

Gene name	Log <sub>2</sub> ratio	P value
Prox1	-2.53	4.11E-04
Gas1	-1.35	8.29E-06
Gas2	-1.34	5.36E-05
Seh1l	-1.35	1.78E-05
Smad6	-1.23	1.72E-04
Ereg	1.13	7.62E-03
Cdk6	1.31	8.00E-05
Tubb3	1.84	1.17E-04
Pdgfb	1.88	1.41E-03
Edn1	2.00	8.52E-06
Cdkn1a	2.16	2.17E-05
Gadd45a	2.23	3.22E-09



**FIGURE 3****A Relative gene expression****B FH-H3.3B ChIP ( $\alpha$ -HA)****C H2A.Z ChIP**